crystals

MDPI

Review

Development of the 2.7 μm to 3 μm Erbium-Doped Laser

Guanghui Liu, Di Gu, Jingliang Liu, Yan Fang, Jiaqi Liu, Zhaoyang Li, Kuofan Cui and Xinyu Chen *

Jilin Key Laboratory of Solid Laser Technology and Application, College of Science, Changchun University of Science and Technology, Changchun 130022, China
* Correspondence: 2010800009@cust.edu.cn

Abstract: The 3 μm wavelength band laser is located on the strong absorption peak of water and the atmospheric transmission window. The 3 μm laser with high single pulse energy is used in medical treatment for cutting soft tissues and bones during surgery. It is used as a pump source for optical parametric oscillators, and Fe lasers can realize 3~5 μm or 8~14 μm laser output, which has an irreplaceable role in certain areas (e.g., optoelectronic countermeasures, LIDAR, atmospheric monitoring, etc.). Commercial semiconductor-pumped Er lasers are capable of achieving 3 μm laser output of 600 mJ with the maturation of a 970 nm semiconductor laser. The conversion efficiency is significantly improved. However, the energy is lower than a flash-lamp-pumped Er laser. There are still serious crystal thermal effects and an inefficient conversion process. In this paper, the energy-level systems of 3 μm Er-doped lasers are discussed. A summary of the current state of research on Er lasers using different matrices and the commercialization of Er-doped lasers with wavelengths ranging from 2.7 μm to 3 μm is also provided. Several technical means are given to enhance laser performance. Furthermore, the development of Er-doped solid-state lasers with wavelengths between 2.7 and 3 μm is envisaged in the near future.

Keywords: Er-doped laser; mid-infrared lasers; 2.7–3 μm

check for updates

Citation: Liu, G.; Gu, D.; Liu, J.; Fang, Y.; Liu, J.; Li, Z.; Cui, K.; Chen, X. Development of the 2.7 μm to 3 μm Erbium-Doped Laser. *Crystals* **2023**, *13*, 1471. https://doi.org/10.3390/cryst13101471

Academic Editor: Stephen J. Cowling

Received: 14 September 2023
Revised: 28 September 2023
Accepted: 4 October 2023
Published: 10 October 2023

Copyright: © 2023 by the authors. Licensee MDPI, Basel, Switzerland. This article is an open access article distributed under the terms and conditions of the Creative Commons Attribution (CC BY) license (https://creativecommons.org/licenses/by/4.0/).

1. Introduction

The Er^{3+} laser has two main bands [1,2]. One of the bands is within the human eye safe range [2] of 1.6 μm. The other band is the 3 μm band, which lies within the strong absorption peak of water [1] and the atmospheric transmission window [3]. Er-doped lasers have an output in the wavelength range around 3 μm, which can be used in medical technology, military applications, industrial processing, atmospheric monitoring [4–9], etc. Due to the continuous development of semiconductor pump sources and crystal growth technology, there has been an increase in demand for conversion efficiency, laser output form, stability, and machine miniaturization for the 3 μm Er laser. As a consequence of the energy level structure of Er ions, it is imperative that the problems of low conversion efficiency and the serious thermal effects of Er crystals be resolved immediately.

Er-doped lasers with a wavelength between 2.7 and 3 μm typically utilize a laser with a wavelength of 970 nm as a pump source, which belongs to a four-energy-level system [10]. The upper and lower energy levels [11,12] of the laser are located in two excited states. The lifetime of the upper laser level ($^4I_{11/2}$) [11] is shorter than that of the lower laser level ($^4I_{13/2}$) [11]. This results in a "self-termination effect" [11–16] of Er^{3+} ion laser transitions in the 3 μm wavelength range. At present, this disadvantage can be overcome by high concentrations of doped activator ions, co-doped de-activator ions, cascades [17–22], etc. As a consequence, it is important to determine the matrix and optimize the ion doping concentration in accordance with the properties of different Er-doped matrix materials.

The working matrices of Er-doped lasers can be divided according to their different compositions and properties. The commonly used matrix materials can be mainly categorized into garnet matrices, fluoride matrices, aluminate matrices, tungstate matrices and sesquioxides [23], etc. Among them, Er:YAG and Er,Cr:YSGG crystals are more widely used

in practical applications. In recent years, research on lasers such as Er:Y_2O_3 ceramics and Er:YAP has gradually increased with the increasing demand for 3 μm laser in various fields. Meanwhile, research into laser gain substances is still expanding. New gain substances such as Er:GGAG have been discovered [24–26]. There are still problems regarding low optical to optical efficiency and serious thermal effects in the existing high single-pulse energy Er laser. This is mainly due to two aspects: (1) the self-termination effect, which results in the pump laser being absorbed by the crystal, meaning that it cannot be fully converted into laser output, and (2) crystal quality, meaning that high-quality laser crystals are required. Although, the existing crystals have serious thermal effects, laser technology is needed to compensate. Sections 3 and 4 will explain these problems and give solutions, respectively.

2. The Applications for Erbium-Doped Lasers

The application of 2.7~3 μm Er-doped lasers is shown in Figure 1. The 3 μm laser within the strong absorption peak of water can be used for laser surgery in the medical field, which is more beneficial to human tissue cutting and blood coagulation than conventional surgery [4,5]. The high-energy single-pulse 3 μm Er laser is used for soft tissue and bone cutting, excision surgery, dental ablation surgery, and cosmetic laser rhytidectomy [4–9]. It is used for cutting and welding materials in the field of industrial processing. The laser in this band is located in the atmospheric transmission window [3] with low propagation losses, which is also suitable for direct use in space science research. In the meantime, the tunable Er laser can be used for atmospheric monitoring [7]. In addition, high-energy 3 μm Er lasers with stabilized pulse outputs can be used as pump sources for 3~5 μm and 8~14 μm optical parametric oscillators [8–12]. They are conducive to the generation of mid- and far-infrared laser outputs, which can have irreplaceable applications in some fields (e.g., in the fields of electro-optical countermeasures, LIDAR, atmospheric monitoring [8–12], etc.). The 3 μm Er laser has always been the focus of research in the field of lasers because of its important applications in the military and civilian fields.

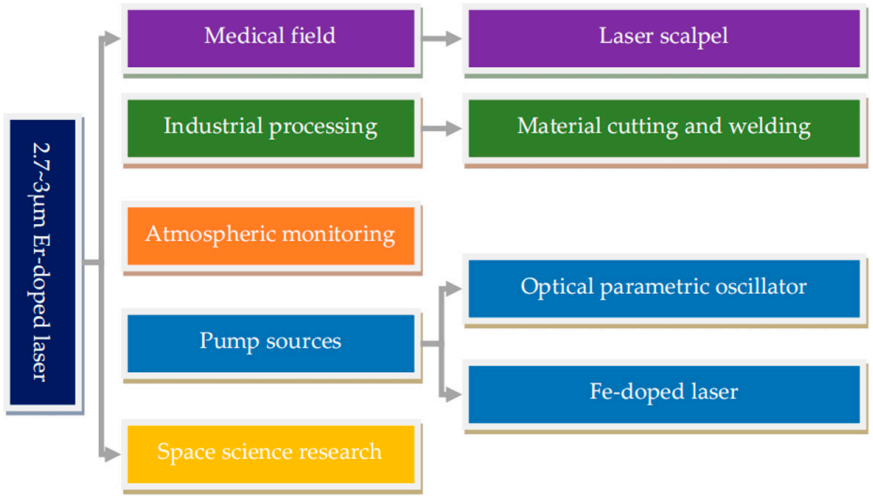


Figure 1. Application of Er-doped lasers with 2.7~3 μm.

The main technologies required to obtain an 2.7~3 μm Er-doped laser include fiber laser technology and the direct output of a rare-earth-ion-doped matrix [27–39]. Laser technology has the advantages of being small in size and lightweight [32]. Among 3 μm fiber lasers, the Er:ZBLAN fiber is the most common [33–35]. In 2018, University Laval in Canada [32] achieved a 41.6 W laser output through using the double-ended pumping of a fusion-free Er:ZBLAN fiber. Further, fiber lasers have made significant progress in ultrashort pulses, wavelength tuning [33–35], etc. Nonetheless, fiber lasers have problems such as low stability, easy damage, and a short service life.

The solid-state waveguide laser is a miniature laser source based on laser material optical waveguides that is compact, stable, and easy to integrate [36–39]. Since light is limited in spatial frequency to the micron range [38,39], the higher optical density of the waveguide reduces the threshold for laser oscillations and increases the slope efficiency of laser outputs. The operating wavelength of Er-doped waveguide lasers [37] is currently 1.55 μm, and the material of the waveguide laser with an operating wavelength of 2.9 μm is Ho:ZBLAN glass [36]. In order to operate a solid waveguide laser [38,39], the gain medium must have a high fluorescence emission line intensity, a high absorption coefficient, and a high fluorescence quantum efficiency. However, the fluorescence quantum efficiency of a 3 μm Er-doped matrix is generally low, and the thermal effect [40] of this material cannot be used as a gain medium for waveguide lasers. In recent years, with the improvement in the quality of crystals, Er:Y_2O_3 [9] as a 3 μm Er-doped matrix shows good thermal performance and high fluorescence quantum efficiency. Perhaps, waveguide lasers with a 3 m wavelength can be used with it as a gain medium.

In contrast, the direct output of a continuous or pulsed 3 μm laser by the Er-doped medium has more advantages, meaning that it is easy to obtain high-power or high single-pulse energy lasers.

3. The 3 μm Er-Doped Laser System

The 3-μm Er-doped laser, which is pumped by a laser near 970 nm, is a four-energy-level system [16]. The energy level transition principle is shown in Figure 2. Er^{3+} ions have a complex upconversion process, self-termination effect, and fluorescence burst during the transition between the $^4I_{11/2}$ [14] and $^4I_{13/2}$ [14] energy levels. These processes lead to low quantum efficiency (theoretically no more than 33.4% [40,41]). This is due to the fact that the upper and lower energy levels are excited states of Er^{3+}, and the upper energy level lifetime is shorter than the lower energy level lifetime.

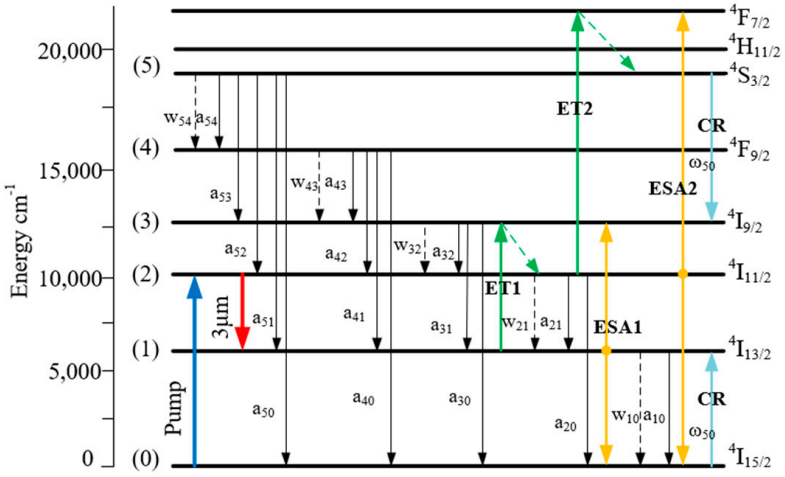


Figure 2. This schematic illustrates the energy level transition for a 3 μm Er−doped laser. a_{ij}—the probabilities of radiation (0, 1, 2, 3, 4 and 5 represent the corresponding energy levels, respectively; i, j = 1, 2, 3, 4, 5); w_{ij}—the probabilities of multiphonon transitions; ω_{50}—cross relaxation rate [14,41].

The upconversion process [42] mainly includes the ground state absorption process ($^4I_{15/2}$ ground state Er^{3+} ions absorb the pump laser near 970 nm to transition to the Stark energy level of the $^4I_{11/2}$ state), excited state absorption process [43] (ESA, Er^{3+} in excited $^4I_{13/2}$ and $^4I_{11/2}$ states absorb pump to transition to higher energy levels, ($^4I_{13/2} \rightarrow {}^4I_{9/2}$) + ($^4I_{13/2} \rightarrow {}^4I_{15/2}$) and ($^4I_{11/2} \rightarrow {}^4F_{9/2}$) + ($^4I_{11/2} \rightarrow {}^4I_{15/2}$)), energy transfer process [43] (ET, $^4I_{13/2} \rightarrow {}^4I_{9/2} \rightarrow {}^4I_{11/2}$, $^4I_{11/2} \rightarrow {}^4F_{7/2} \rightarrow {}^4S_{3/2}$), and cross-relaxation process (CR, ($^4I_{15/2} \rightarrow {}^4I_{13/2}$) + ($^4S_{3/2} \rightarrow {}^4I_{9/2}$)) [41–45]. In addition, particles in the excited state undergo radiation-less chirping to lower energy levels. The energy transfer process is enhanced by increasing the Er^{3+} doping concentrations. ET1 and ESA1 processes promote $^4I_{13/2}$ energy

level emptying while replenishing $^4I_{11/2}$ energy level particles and partially inhibit the self-termination effect [45,46]. The particles in the upper level will transition downward to produce a laser if the inversion population distribution is formed in both the upper and lower energy levels [4]. In the resonant cavity, the light intensity distribution is uneven. As the working state of the laser stabilizes, the output performance can be characterized by some important indicators [12], including output power, FWHM [4], bandwidth, etc. The output power is the energy of the laser per unit time. FWHM is the half-wave width of a single laser pulse. Bandwidth [20] is the frequency tuning range of the laser.

The Er^{3+} doping concentration and the choice of matrix determine the energy level lifetimes [47]. The energy level lifetime determines the laser's efficiency and limits the form of laser output. Large differences in the lifetimes of the $^4I_{11/2}$ and $^4I_{13/2}$ energy levels of some matrices and serious self-termination effects make it difficult to realize high-power continuous-wave laser output [40]. Despite this, pulsed pumping can be used to produce long pulsed laser outputs. The conversion efficiency [48] is still low. In this regard, it is imperative to design crystals carefully. Studying the upconversion process [43] and the self-termination effect [15] enables the gain-matching of the self-termination effect with the lifetime of the upper energy levels. Designing a pump laser to optimize pump storage can effectively improve conversion rates.

In addition, the Er^{3+} energy level splits into the multiple Stark energy level in the presence of the crystal field of its doped matrices, which will lead to some differences in the output characteristics of Er^{3+} doping at diverse doping concentrations and in different laser media.

4. Development Status of 3 μm Er-Doped Laser Media and Their Lasers

The matrix material determines the physical, chemical, and mechanical properties of the Er^{3+} ion-doped active medium [23]. The main matrix materials for Er^{3+}-doped active medium are garnet, fluoride, sesquioxide and aluminate crystals, etc. [40]. This section will focus on the development status of Er-doped lasers that utilize commonly used matrix materials as active media. Table 1 summarizes the main physical parameters of a commonly used Er-doped matrix.

Table 1. Physical parameters of a commonly used Er-doped matrix.

Active Medium	T [K]	α [10^{-6}K]	κ [W·m^{-1}K^{-1}]	Δn	Ph [cm^{-1}]	References
Er:YAG	1970	8.2	11.72	-	865	[49]
Er:YSGG	1877	-	6.83	-	728	[50]
Er:YLF	830	13	6	0.0227	447	[2]
Er:SrF_2	1473	18.4	8.3	-	280	[7]
Er:CaF_2	1418	18.9	9.7	-	322	[51]
Er:YAP	1875	9.5	11	0.0235	550	[52]
Er:Y_2O_3	2430	8.5	13.4	-	597	[49]
Er:Lu_2O_3	2450	8.6	12.8	-	618	[49]

T—melting point; α—coefficient of thermal expansion; κ—thermal conductivity; Δ*n*—birefringence; Ph—phonon energy.

4.1. Development Status of Er-Doped Garnet Crystals and Their Lasers

Garnet hosts have a cubic structure with O_h^{10} space groups. Garnet crystals have good mechanical properties and can be readily obtained. As part of this group, YAG crystals and YSGG crystals are widely represented and widely used [47,53]. Er:YAG crystals have high thermal conductivity [49] (11.72 W/(cm·K)) and excellent thermal properties [50]. Regarding their laser, as a result of its high phonon energy [49] (865 cm^{-1}) and multi-phonon quenching effect, the upper level lifetime is much shorter than the lower level lifetime. It is not conducive to the realization of particle number inversion, resulting in a higher laser threshold. In contrast, Er:YSGG crystals have a longer upper energy level

lifetime (1.58 ms) [47], which is beneficial to achieving particle number inversion. However, the thermal conductivity is low (6.83 W/(cm·K)) [50], and the thermal effect is more serious.

4.1.1. Er:YAG

The output wavelengths of Er:YAG crystals doped at various concentrations are different. Moreover, 0.5~50 at.%-doped Er:YAG crystals can realize laser outputs of 1.6 μm, 2.7 μm, or 2.94 μm [54–58]. Low-concentration-doped Er:YAG crystals produce a laser output of 1.6 μm [53], and they can achieve 1.6 μm and 2.7 μm cascade laser outputs under cryogenic cooling [54] and produce 1.5 μm and 2.94 μm cascade laser outputs at room temperature [55]. In 2022, Wang et al. pumped 10 at.%- and 25 at.%-doped Er:YAG crystals with a 976 nm diode and achieved cascade laser outputs of 1469 nm and 2937 nm at room temperature [56]. The output slope efficiencies of the mid-infrared laser at a wavelength of 2937 nm were measured to be 37.2% and 36.5%, respectively [56]. Both broke the Stokes limit. With a 30~50 at.% high doping concentration, Er:YAG crystals with an output wavelength of 2.94 μm are currently the only active medium capable of directly outputting a 2.94 μm laser [57,58].

In 1967, E. V. Zhavikov and his colleagues were the first to use Er^{3+}-doped garnet as an active medium for a laser. They used a flash lamp to pump a 30 at.% Er:YAG crystal to obtain a laser with an output wavelength of 2940 nm at room temperature. In 1990, S. Wuthrich [59] obtained a pulse energy of 400 mJ by pulse pumping a 40 at.% Er:YAG crystal with a flash lamp. Without Q-switching, pulse durations were in the hundreds of microseconds or even milliseconds [59]. Flash-lamp-pumped laser systems are more effective at producing high-energy single pulses. In comparison to diode-pumped laser systems, flash-lamp-pumped laser systems display a lower optical conversion efficiency. Thus, Chen et al. [60] were the first to polarization couple two semiconductor lasers (wavelengths of 963.7 nm and 964.2 nm, respectively). They achieved the end-face pumping of Er:YAG crystals with a 50 at.% doping concentration [60], as shown in Figure 3a, and a 2.94 μm laser output with a power of 1.15 W and a slope efficiency of 34% was obtained [60] in 1999. In 2010, JG Sousa [61] realized a highly efficient and compact diode laser pumping 2.94 μm Er:YAG laser with an energy of up to 9 mJ [61]. The semiconductor technology in this period was still immature, so flash lamp pumping was still the main method to obtain a high-energy laser output. In 2004, Zajac A [5] developed a lamp side-pumped Er:YAG electro-optic Q-switched 2.94 μm laser for medical use. It is shown in Figure 3b. It obtained a single pulse output with a pulse width of 91.2 ns and a maximum output energy of 137 mJ on the basis of the electro-optic Q-switching of $LiNbO_3$ crystal [5]. In 2014, Yang et al. [62] presented an electro-optic Q-switched high-energy Er:YAG laser with two polarizers. It is shown in Figure 3c [62]. They used two Al_2O_3 polarizing plates and a $LiNbO_3$ crystal with a Brewster angle. A pulse energy of 226 mJ and a pulse width of 62 ns were obtained by optimizing the tuning Q delay and thermal compensation [62]. In 2021, Karki Krishna [63] pumped 50 at.% Er:YAG with a flashlamp and rotating mirrors to develop a mechanically Q-switched laser. It is shown in Figure 3d. A 2.94 μm laser output with a maximum output energy of 805 mJ, a pulse width of 61 ns, and a repetition frequency of 1 Hz was obtained [63]. A commercial Er:YAG laser excited by flash lamp pumping has also been established. It is capable of achieving a 2.94 μm laser output, along with a maximum pulse energy of 3 J, at low heavy frequencies. In recent years, semiconductor lasers with a wavelength of 970 nm have been developed gradually. In 2016, Pantec successively introduced 970 nm high-energy diode modules [64] that greatly contributed to the development of high single-pulse energy 3 μm Er-doped lasers. Diode-pumped Er:YAG and Er,Cr:YSGG lasers have been successfully commercialized to achieve pulse outputs with a maximum energy of 600 mJ. For example, a diode-pumped Er:YAG continuous laser with 1 W output power has been established. In 2016, Manuel Messner et al. showed a 50 at.% Er:YAG laser pumped by a high-energy diode with an average output power of up to 50 W [64]. At present, the diode-pumped Er:YAG laser has not broken through the limitation of the laser upper level lifetime to achieve a high power or high energy laser output [65].

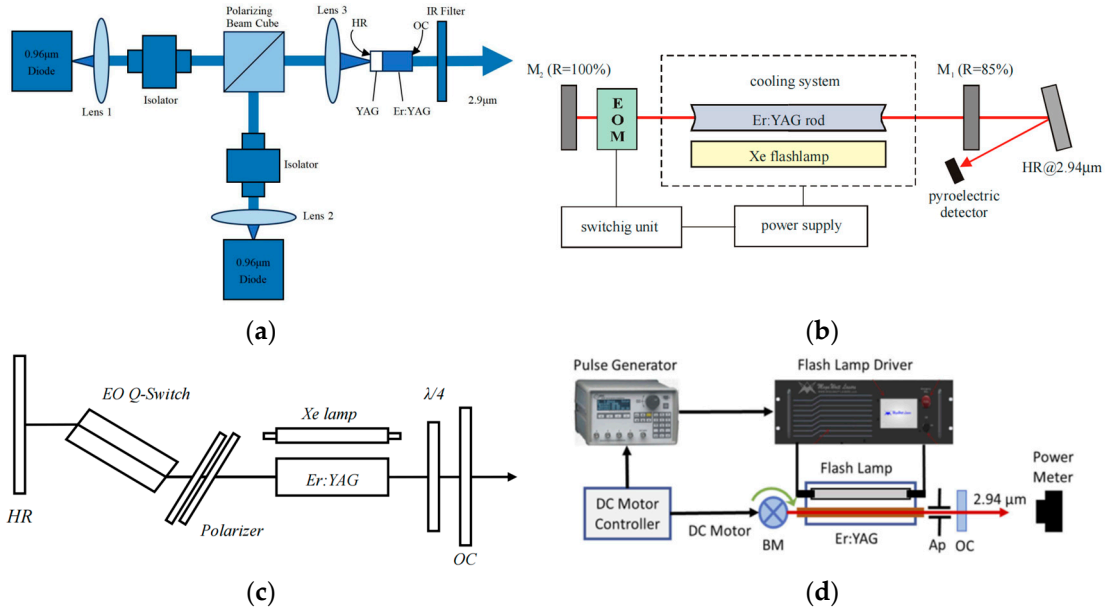


Figure 3. (**a**) Diode-pumped Er:YAG laser [60].; (**b**) lamp side-pumped Er:YAG electrooptically Q-switched laser [5]; (**c**) lamp side-pumped Er:YAG two-polarizer high-power electrooptically Q-switched laser [62]; (**d**) mechanically Q-switched Er:YAG laser [63].

The 3 μm Er-doped laser can be used as a pump source for the Fe laser [66,67], which is favorable for generating a 4~5 μm laser output [4,5,7,68]. So, the main requirements for Er laser systems are compactness, stability, a high output energy, and efficiency. The best way to obtain a high energy output is flash side-pumping. However, this has the disadvantages of low efficiency and instability. In 2019, Li et al. [66] achieved a 2.93 μm laser output with a maximum pulse energy of 1.414 J using flash-lamp-pumped Er,Cr:YAG. It was the first time that Fe:ZnSe was pumped at cryogenic cooling and room temperature [66]. In 2021, Dmitry Martyshkin et al. [67] used a mechanically Q-switched flash-lamp-pumped Er:YAG laser with a maximum output energy of 220 mJ as a pump source. It was amplified by a three-stage power amplifier with maximum output energies exceeding 60, 56, and 48 mJ at 4.4, 4.3, and 4.1 μm, respectively [67].

Er:YAG crystals have been pumped by flashlamps to achieve laser outputs at high single-pulse energies, which are accompanied by severe thermal effects that affect the laser output performance. In order to reduce thermal effects under high-power pumping and further improve output optical performance, designing diode-pumped Er: YAG lasers could help to overcome the limitations of energy level lifetimes and improve the thermal management of crystals to realize high conversion efficiency and high single-pulse energy laser output.

4.1.2. Er:YSGG

In 1994, Dinerman et al. reported a continuous laser output with a power of 511 mW at 2.79 μm from a laser diode-pumped Er:YSGG crystal [13]. Due to the serious thermal phenomenon of Er:YSGG crystals, researchers have improved laser performance via the thermal management of crystals. In 2013, E. A. Arbabzadah [69] obtained pulse energies of up to 55 mJ and sloped efficiencies of 20.5% with 50 at.% Er:YSGG (Figure 4a) [69]. In 2015, Wang [70] diode-pumped 30 at.% Er:YSGG with an average output power of 10.1 W and a slope efficiency of 6.5% was obtained by compensating the thermal lens to obtain a laser output with a pulse energy of 562 mJ at 16 Hz, and the device is shown in Figure 4c [70]. In 2019, Chen [71] used a 968 nm LD side-pumped 35% Er:YSGG laser with TeO_2 as an acousto-optic Q-switch. It is shown in Figure 4b. It can output a laser with a single pulse energy of 2 mJ and a pulse width of 63.18 ns at a frequency of 500 Hz [71]. This was equivalent to an average output power of 10 W. In the same year, Hu et al. [72] realized

a 2.8 μm laser output with a maximum slant efficiency of 31.5% and a maximum output power of 0.75 W. This is the highest reported slant efficiency of Er:YSGG crystals for the 2.8 μm output at present [72]. In 2022, Ye [73,74] used a diode-side-pumped Er^{3+} ion-doped crystal of double-bar Er:YSGG with a doping concentration of 35 at.%, and the device is shown in Figure 4d. The maximum output power that could be obtained was 61.02 W [74], and the optical to optical conversion efficiency was 12.6% of 2.8 μm laser output [74]. In 2022, V. P. Mitrokhin et al. [75] achieved a maximum output energy of over 0.8 J for the first time in the free running state that used diode-pumped Er, Cr: YSGG crystals [75]. The peak power of the output laser pulsed with a duration of 55 ns in the case of an active Q-switch exceeded 1 MW, and the energy was stable. It was also possible to pump Fe:ZnSe crystals as a pump source and realize a pulsed laser output of 4.2 μm [75]. A commercially available flash-lamp-pumped Er,Cr:YSGG laser achieved a 2.79 μm laser output with a maximum pulse energy of 1.8 J at low heavy frequencies (1–20 Hz) [53,54,76]. Er:YSGG crystals exhibit excellent properties in high-frequency laser or continuous-wave lasers.

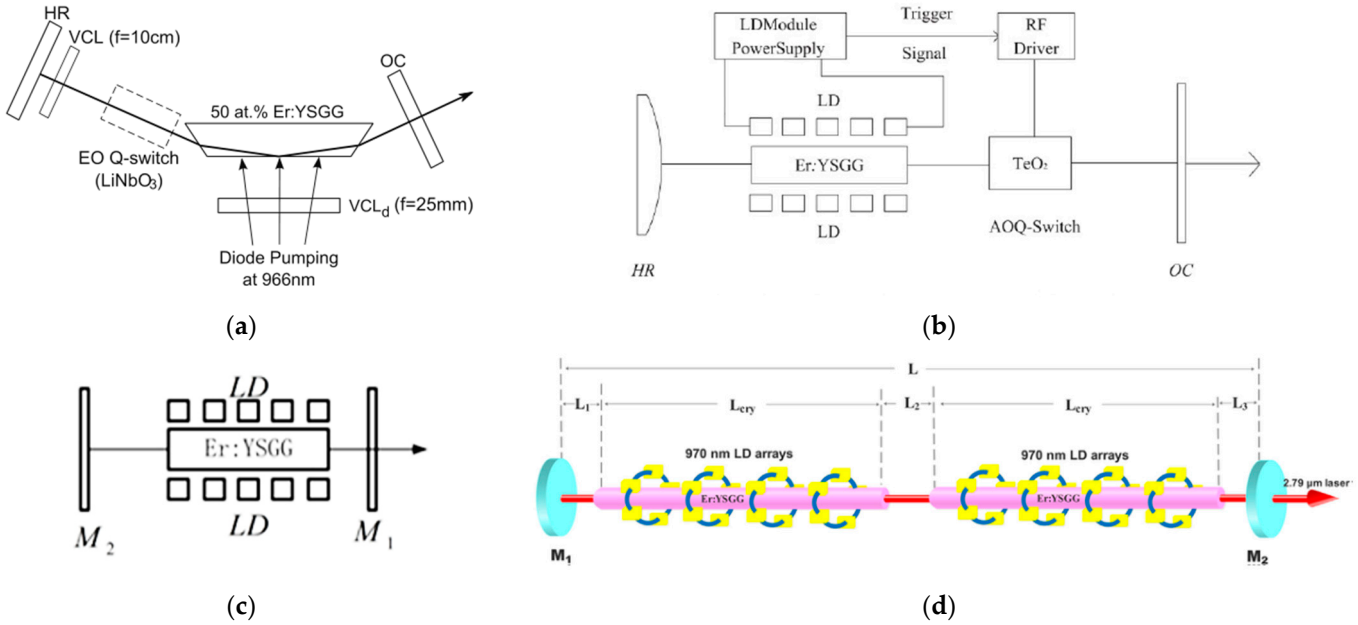


Figure 4. (**a**) Diode-pumped surface-cooled Er:YSGG electrooptically Q-switching laser [69]; (**b**) high heavy-frequency Er:YSGG laser [71]; (**c**)diode-side-pumped Er:YSGG continuum laser. Reprinted with permission from Ref. [70]; (**d**) diode-side-pumped two-rod Er:YSGG laser [74].

4.2. Development Status of Er-Doped Fluoride Crystals and Their Lasers

Common fluoride matrices doped with Er^{3+} ions in the 3 μm band include Er:CaF_2, Er:SrF_2, and Er:YLF crystals [77]. The Er^{3+} doping concentration required for Er:SrF_2 and Er:CaF_2 crystals is relatively low. Their concentrations range from 1.7 at.% to 5 at.% [78–90]. Er:YLF crystals commonly have an Er^{3+} doping concentration of 15 at.% [91–103]. Compared with garnet crystals, fluoride crystals have lower phonon energies [2,7,51,82,83,86] (447 cm^{-1}; 280 cm^{-1}; 322 cm^{-1}) that help to reduce the non-radiative transition and multi-phonon relaxation probability between energy levels. This results in a reduction in the laser threshold and an increase in efficiency. Er:YLF crystals have birefringence and a negative refractive index thermo-optic coefficient, meaning that the thermal lens effect is small and that the thermal stability is high [2]. Er:SrF_2 and Er:CaF_2 crystals have unique crystal structures that result in wide emission spectra [7,51,82,83,86]. However, fluoride crystals are fragile and difficult to process.

4.2.1. Er:SrF_2 and Er:CaF_2

In 1967, Robinson et al. achieved the first mid-infrared laser output in the 2.69 μm band by using a flash-lamp-pumped CaF_2:ErF_3:TmF_3 (79%:20.5%:0.5%) [78]. In 1989, S.a. Pollack et al. reported the first continuous-wave Er:CaF_2 laser at 2.7 μm pumped by a flash lamp laser output [79]. In 2006, T. T. Basiev et al. realized a 2.75 μm continuous laser output of a transverse diode-pumped Er:SrF_2 and Er:CaF_2 [80]. In 2013, J. Šulc et al. found that Er:CaF_2 output laser wavelengths were tuned in the range of 2687–2805 nm. It took the value of 118 nm [81]. In 2018, Richard Švejkar found the Er:SrF_2 output laser wavelength tuning range of 123 nm in 2690 nm—2813 nm [7]. Because of their wide emission spectrum, they might be used to generate ultrashort pulses. In the same year, Fan obtained a continuous-wave laser output of 1.06 W with a slope efficiency of 41%, a pulsed laser output of 12.1 μJ, along with a passive Q-swiching of ReS_2 of 508 ns by using an Er:SrF_2 crystal [82]. In 2022, Zhao et al. successively realized a continuous-wave laser output of 2.32 W and a pulsed laser output of 0.49 mJ, with a pulse width of 555 ns, by using Er:CaF_2 [83]. The matrix thermal expansion coefficients and electrical conductivity coefficients of Er:SrF_2 and Er:CaF_2 crystals indicate that they are not suitable for use as an active medium for high-power or high-energy laser [87]. However, their large wavelength tuning range and high conversion efficiency at low power are suitable for some applications [87–90].

4.2.2. Er:YLF

Er:YLF crystals are in the C_{4h}^6 space group; they have tetragonal crystal structures and are optically anisotropic. These crystals are capable of outputting linearly polarized lasers [2,91,92].

In 1987, G.J. Kintz longitudinally pumped 8% Er:YLF with a 797 nm multistrip laser diode array, and the first 2.8 μm laser output of Er:YLF was observed [2]. In 1995, T. Jensen [93] first reported a 970 nm diode-pumped Er:YLF. It achieved a maximum continuous-wave output power of 1.1 W and a 35% slope efficiency. In 1997, Wyss achieved a laser output with a slant efficiency of 50% by pumping Er:YLF with a titanium gemstone laser [94], higher than quantum efficiency. The device is shown in Figure 5a. In 2003, Alex Dergachev and Peter F. Moulton obtained a continuous laser output of 2810 nm at 4 W by diode pumping Er:YLF [95]. It realized 2720–2840 nm tuning at 11 different wavelengths. In 2012, M. V. Inochkin [96–99] used Fe:ZnSe crystals for Q-switching, and the device is shown in Figure 5b. It obtained a 2.81 μm laser output of 3 mJ and a pulse width of 30 ns [96–99]. In 2018, Manuel Messner proposed a new diode-side-pumped Er:YLF scheme [91]. The device is shown in Figure 5c. It achieved an output power of greater than 10 W average output power, along with a single pulse energy of more than 100 mJ and a high slope efficiency of 18.7% [91], and the diode multidimensional side-pumping method effectively moderated the thermal effect and improved the conversion efficiency. In the following year, acousto-optic Q-switching was carried out on this basis [100], and a 2.81 μm laser output with an output optical peak power of 50 kW, a pulse width of 70 ns, and an energy of 3.5 mJ was obtained at a high frequency of 100 Hz [100]. In 2019, Nikolay Ter-Gabrielyan and Viktor Fromzel realized cascade laser outputs of 2.8 μm, 1.73 μm, and 1.62 μm [101]. The device is shown in Figure 5d. In 2021, A. V. Pushkin obtained a laser output with a pulse width of 13 ns, an output energy of 82 mJ, and a wavelength of 2.67 μm by using electro-optic Q-switching with a KTP crystal at a repetition frequency of 20 Hz [103]. The average output power was watt-scale at 50 Hz frequency, and the wavelength could be tuned in 2667–2851 nm. Er:YLF crystals exhibit excellent optical properties [103]. These types of crystals can be used as a high single-pulse energy active medium, with a wide wavelength tuning range at the watt level.

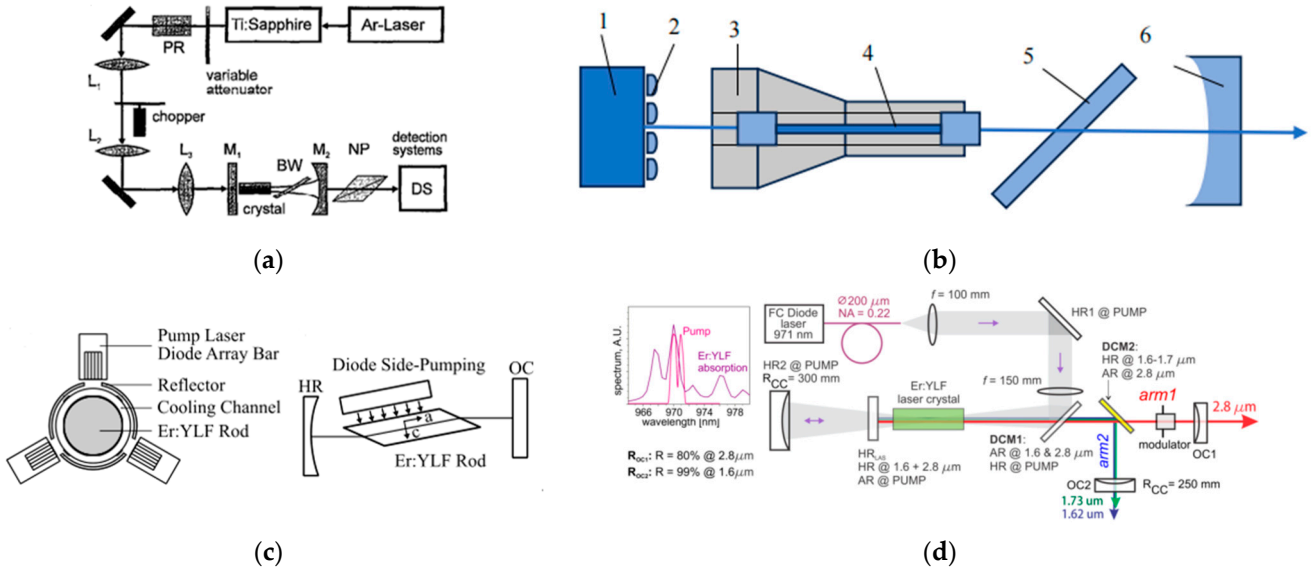


Figure 5. (**a**) Ti/sapphire laser-pumped Er:YLF laser. Reprinted with permission from Ref. [94]; (**b**) Fe^{2+}:ZnSe Q-switching miniature Er:YLF laser (1—array of laser diodes; 2–microscope lenses; 3–total-internal-reflection prism; 4–Er:YLF; 5–Fe^{2+}:ZnSe shutter; 6—spherical output mirror with radius of curvature r = 1.2 m) [98]; (**c**) new diode-side-pumped Er:YLF laser [91]; (**d**) 2.8μm Er:YLF Q-switching cascade laser [101].

4.3. Development Status of Er-Doped Sesquioxide Crystals and Their Lasers

Sesquioxide crystals have higher thermal conductivity, a lower phonon energy [48] (about 600 cm^{-1}), wider gain spectral band, higher anti-laser damage threshold and quantum efficiency, and uniform thermal stress and induced birefringence compared to garnet oxide crystals [93]. Therefore, sesquioxide crystals are ideal matrix materials for high-power and ultra-short pulse lasers. It should be noted, however, that sesquioxide crystals have a high melting point [48] (about 2400 K), making crystal preparation difficult.

4.3.1. Er:Y_2O_3

In 2010, Diode-pumped cryogenically cooled 2 at.% Er:Y_2O_3 ceramic lasers [9] were first reported by T. Sanamyan et al. in the U.S. The device is shown in Figure 6a. It obtained a 2.71 μm quasi-continuous-mode laser output with a power of more than 1.6 W and a slope efficiency of 27.5% [104]. In the following year, they obtained a continuous output of 14 W at low temperatures, with a slant efficiency of about 26% [105]. In 2016, they boosted the power to 24 W [106]. In 2015, they achieved the first cascaded dual-wavelength continuous-wave output of diode-pumped 0.5 at.% Er:Y_2O_3 cryogenic ceramics [107]. The device is shown in Figure 6b. The cascaded dual-wavelength continuous-wave outputs in the 1.6 μm and 2.7 μm can output 24 W and 13 W with slant efficiencies of 38% and 26%, respectively [107]. In 2017, Wang achieved a 2.7 μm continuous laser output of 2.05 W at room temperature by using 7 at.% concentration of Er:Y_2O_3 ceramic as a gain medium for lasing [108]. In 2022, Ding reported the generation of a 13.4 W continuous-wave laser output at room temperature with a slope efficiency of 16% [109]. This was based on a homemade high-optical-quality ceramic sample. The device is shown in Figure 6c. This is the highest output power achieved by a laser diode-pumped 3 μm erbium-doped ceramic laser [109]. In addition, Er:Y_2O_3 mode-locking of the laser showed good results. In 2018, Qin et al. realized a passively Q-switched Er:Y_2O_3 ceramic laser by utilizing SESAM as SA; it produced a 1.7 μJ pulse at 2709.3 nm energy and a 350 ns pulse duration [110].

4.3.2. Er:Lu_2O_3

In 1998, V. Peters first experimentally pumped 3% Er:Lu_2O_3 with a 973 nm LD to obtain a 3 μm area laser output with an output power of 3 W [111]. In 2012, Li T achieved a

continuous optical output of diode-pumped Er:Lu_2O_3 at room temperature with an output power of 1.7 W at a wavelength of 2.84 μm and a slanting efficiency of 11% [112]. In the same year, the power was boosted to 5.9 W, with a slant efficiency of 27% [113]. In 2020, Yao [114] proposed a high-power and high-efficiency laser diode-pumped Er:Lu_2O_3 ceramic laser. It had a continuous-wave output power of 6.7 W at 2845 nm and a slope efficiency of 30.2% [114]. This is the highest slope efficiency achieved for a laser diode-pumped 3 μm erbium-doped ceramic laser [114]. Compared with the Y_2O_3 crystal, the Lu_2O_3 crystal has poor performance as a continuous-wave laser working material. For mode-locked lasers, however, it has shown good performance. In 2018, Wang et al. [115] realized a passively Q-switched Er:Lu_2O_3 ceramic laser by using SESAM as SA. The device is shown in Figure 6d. It had a pulse energy of ~9.8 μJ and produced pulses with a duration of 70 ns [115]. In 2019, H Uehara obtained a 2845 nm laser output with a pulse duration of 247 ns and a maximum pulse energy of 9.4 μJ by using a monolayer graphene saturable absorber to passively Q-tune the Er:Lu_2O_3 ceramic laser [116].

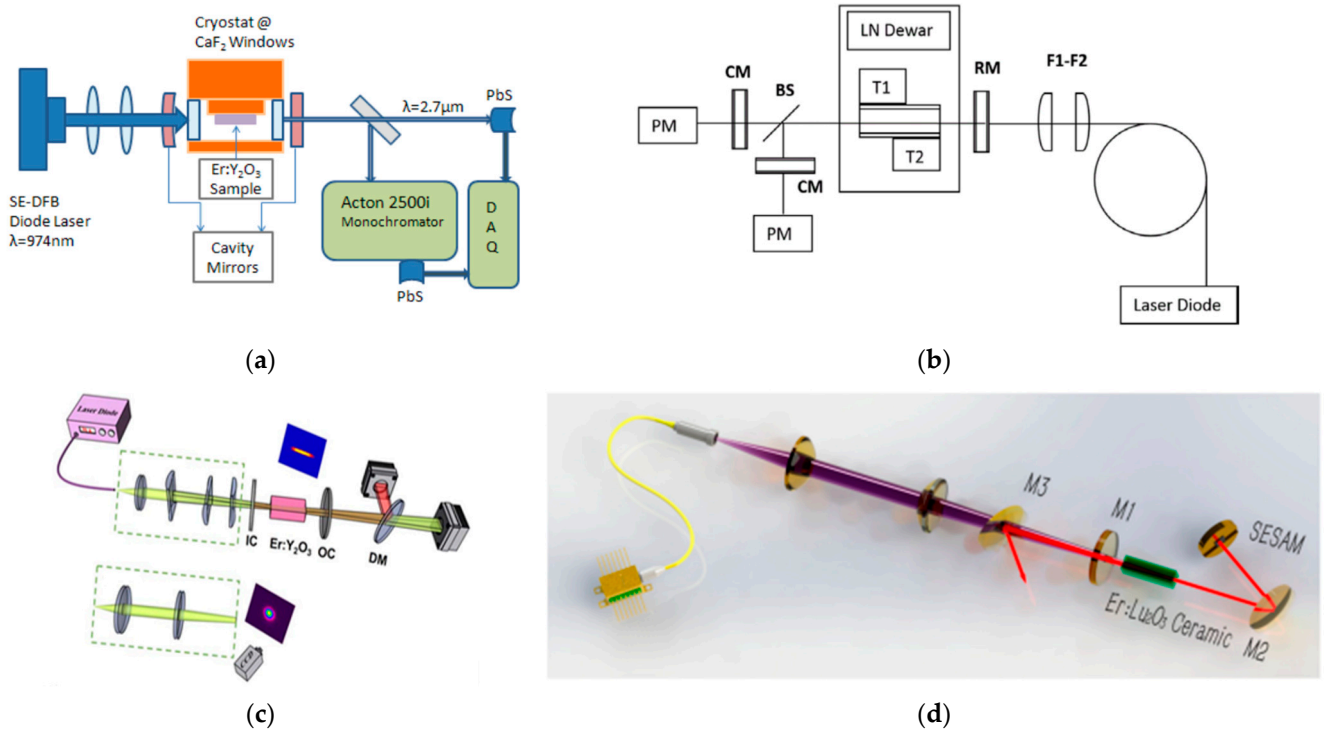


Figure 6. (**a**) Diode-pumped cryo-cooled Er:Y_2O_3 ceramic laser [9]; (**b**) Er:Y_2O_3 cryo-cooled ceramic cascade laser. Reprinted with permission from Ref. [107]; (**c**) Er:Y_2O_3 ceramic laser [109]; (**d**) passively Q-switching short-pulse Er:Lu_2O_3 ceramic laser [115].

4.4. Development Status of Er-Doped Aluminum Crystals and Their Lasers

Er:YAP crystals are orthorhombic crystal structures with a D_{2h}^{16} space group. They have thermodynamic and mechanical properties similar to those of YAG crystals [40] (9.5 $\times 10^{-6}$ K, 11 W·m^{-1}K^{-1}). Furthermore, in comparison with YAG crystals, they also have excellent thermal conductivity, low phonon energy (550 cm^{-1}) [51], negative biaxial crystals, optical anisotropy, and excellent natural birefringence. They are suitable for obtaining higher-power polarized laser outputs [40,117,118]. In addition, Er:YAP crystals have a lower melting point than sesquioxide crystals and are easier to prepare. Commonly, 10 at.%-doped Er:YAP crystals have an output wavelength of 2.7 μm [119,120], and 5 at.%-doped Er:YAP crystals have an output wavelength of 2.92 μm [121,122].

In 1976, A.A. Kaminski first proposed that Er:YAP media were suitable for generating a polarized laser radiation of about 3 μm [40]. In 1987, M. Stalder and W. Lüthy measured the polarization characteristics of the 3 μm-band laser output from Er:YAP [117]. In 1990,

Zeng pumped Er:YAP crystals with a flash lamp and obtained a 2.7 μm laser output of 249 mJ [118]. In 2018, Richard Švejkar achieved the first 2.7 μm laser output using diode-pumped Er:YAP crystals at low temperatures and a slope efficiency of 3.5% [119]. In the same year, Quan realized a dual-wavelength output of 2710 nm and 2728 nm at room temperature [120]. The device is shown in Figure 7a. It obtained 739 mW and 738 mW laser outputs under continuous-mode and pulsed-mode diode pumping, respectively. They had slope efficiencies of 12.1% and 13.8%, respectively [120]. In 2019, HIROKI KAWASE obtained a continuous-wave laser output at 2920 nm wavelength with 0.674 W and a slope efficiency of 31% at room temperature [121]. In the same year, a 2.9 μm laser output of 5.1 μJ at 460 ns was realized via the use of a monolayer graphene saturable absorber [122]. The device is shown in Figure 7b. Yao achieved the first dual-wavelength output at 2.73 μm and 2.80 μm using a Rhenium diselenide ($ReSe_2$) Q switch. Its maximum output power was 526 mW [123]. In the following year, Yao obtained a continuous-wave output of 6.9 W at 2920 nm with a slope efficiency of 30.6% [124]. The device is shown in Figure 7c. In 2022, Yao proposed a 2.9 μm Er:YAP laser with a scaled output power via dual-wavelength pumping [125]. The device is shown in Figure 7d. This laser had 976 nm and 1.7 μm pump wavelengths. It showed an increase in power compared to a single-wavelength pump [125,126].

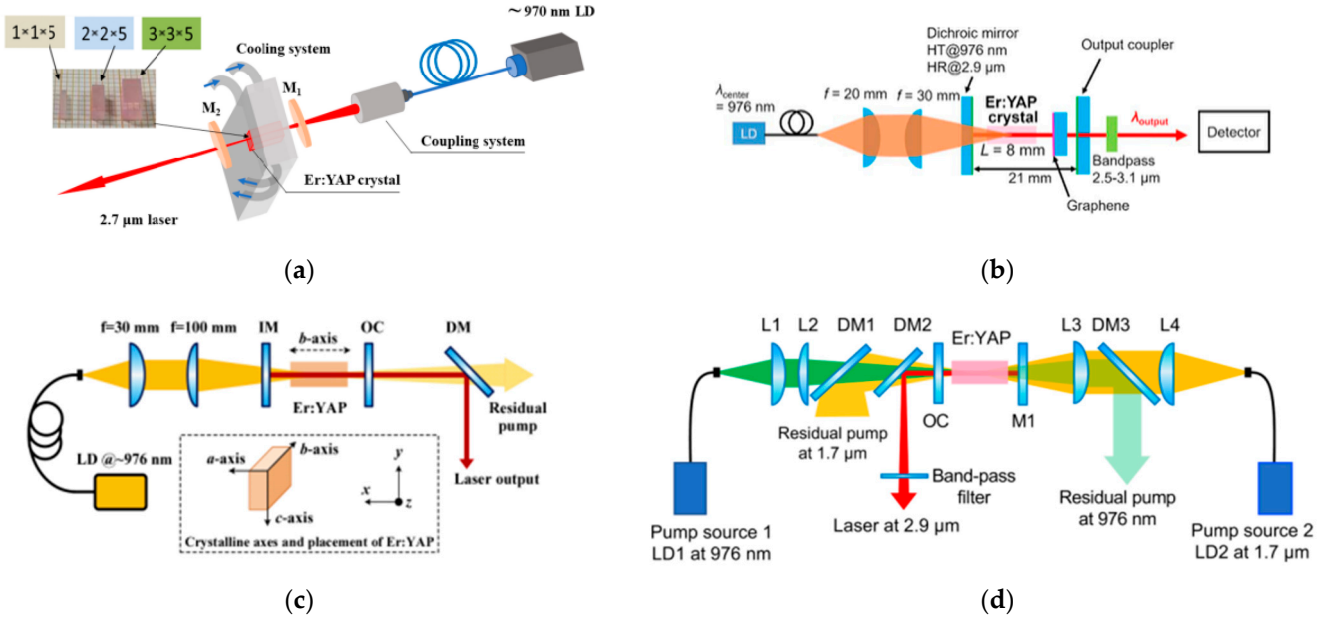


Figure 7. (**a**) Diode end-pumped dual-wavelength Er:YAP laser [120]; (**b**) monolayer graphene saturable absorber Er:YAP pulsed laser. Reprinted with permission from Ref. [122]; (**c**) high-efficiency Er:YAP laser [124]; (**d**) dual-wavelength-pumped 2.9 μm Er:YAP laser. Reprinted with permission from Ref. [125].

This section summarizes the current status of the development of 3 μm Er-doped laser media and their lasers; overall, Er:YSGG and Er sesquioxide crystals are ideal active media for high-power continuous-wave lasers. High single-pulse energy outputs can be achieved through using Er:YAG, Er, Cr:YSGG, and Er:YLF crystals [127–130]. On the other hand, Er-doped laser media generally suffer from serious thermal effects and low conversion efficiency. The many ways in which the above studies aimed to enhance laser performance can be summarized as follows: (1) Optimizing the Er ion doping concentration and crystal configuration in the matrix. (2) Designing diode arrays for matrices that absorb high-power pumps accompanied with severe thermal effects (the diode array is designed by using multi-dimensional ring pumping and pumping light delivery more uniformly, which improves the quality of the output beam and reduces the thermal load on the components).

(3) Designing the pump light to optimize pump energy storage can effectively improve the conversion efficiency. (4) Selecting a suitable modulation device to further compress the pulse width with the help of electro-optical Q or mechanical Q, etc.

5. Conclusions and Outlook

In summary, the direct output of 3 μm lasers from Er-doped media is more beneficial in high-power operation or high single-pulse energy operation, which is better than fiber laser technology. This paper summarizes the output characteristics of different Er-doped matrices and the current status of laser research. Tables 2 and 3 summarize important conclusions about Er-doped lasers. Several studies have demonstrated excellent performance for high single-pulse energy lasers using Er:YLF and Er:YAG matrixes. In the case of continuous-wave lasers, Er:YSGG, Er:YAP, and Er-doped sesquioxide are ideal active mediums. Er:SrF_2 and Er:CaF_2 crystals are not suitable as matrices for high-power or high-energy lasers. Despite this, they are able to produce high conversion efficiencies at low power levels and have an extensive wavelength tuning range. With the development of a 970 nm semiconductor laser, flash lamp pumping has been gradually replaced by diode pumping. High single-pulse energy Er-doped lasers still suffer from low conversion efficiencies and some thermal effects. On the other hand, laser performance can be effectively enhanced via the of optimization of the Er ion doping concentration and crystal configuration in the matrix, the design of pump light, Q-switching, etc.

Table 2. Important conclusions for continuous-wave Er-doped lasers.

Active Medium	Er Conc. (at.%)	Pump	P_{out} (W)	σ (%)	λ (μm)	References
Er:YAG	50	LD	1.5	34	2.94	[60]
	50	LD	50	-	2.94	[64]
Er:YSGG	30	LD	0.75	31.5	2.8	[72]
	35	LD	61.02	12.6	2.8	[74]
Er:SrF_2	3	LD	1.3	9.2	2.69–2.813	[7]
Er:CaF_2	1.7	LD	2.32	-	2.75	[83]
Er:YLF	15	LD	1.1	35	2.8	[93]
	15	Sapphire	-	50	2.8	[94]
	15	LD	10	18.6	2.8	[91]
Er:Y_2O_3	2	LD	1.6	27.5	2.7	[104]
	0.5	LD	13	26	2.7	[107]
Er:Lu_2O_3	11	LD	6.7	30.2	2.85	[114]
Er:YAP	10	LD	0.74	12.1	2.7	[120]
	5	LD	6.9	30.6	2.92	[124]

P_{out}—output power, σ—slope efficiency, λ—emitted laser wavelength.

Table 3. Important conclusions for pulsed Er-doped lasers.

Active Medium	Er Conc. (at.%)	Pump	f (Hz)	τ_{pulse} (ns)	E_{pulse}	λ (μm)	References
Er:YAG	50	flash lamp	1	61	805 mJ	2.94	[63]
Er:YSGG	35	LD	500	63.18	2 mJ	2.79	[71]
Er:SrF_2	3	LD	49 k	508	12.1 μJ	2.79	[82]
Er:CaF_2	1.7	LD	500	555	0.49 mJ	2.75	[83]
Er:YLF	15	LD	20	13	82 mJ	2.67	[103]
Er:Y_2O_3	7	LD	130.6 k	350	1.7 μJ	2.7	[110]
Er:Lu_2O_3	7	LD	71 K	70	9.8 μJ	2.7	[115]
Er:YAP	5	LD	114 k	460	5.1 μJ	2.94	[122]

F—frequency, τ_{pulse}—pulse width of emitted laser, E_{pulse}—energy of emitted laser, λ—emitted laser wavelength.

There are still some challenges that need to be examined in the future. Firstly, the selection and preparation of high-quality Er-doped crystals with high thermal conductivity and low phonon energy need to be carried out to meet the needs of high-power 3 μm laser operation with high efficiencies or high single-pulse energies. Secondly, high-damage threshold optics and electro-optic Q-modulation crystals are also required to achieve high single-pulse energy laser outputs. Finally, there are various types of Er-doped lasers, such as high-power continuous-wave lasers, wavelength-tunable lasers, and mode-locked lasers. They will also need to meet the needs of different fields in practical applications with the development of different Er-doped matrix growth technologies.

Author Contributions: Conceptualization, G.L., J.L. (Jingliang Liu) and Y.F.; investigation, G.L., J.L. (Jiaqi Liu), Z.L. and K.C.; visualization, G.L.; writing—original draft, G.L. and D.G.; writing—review and editing, G.L.; validation, X.C. and J.L. (Jingliang Liu); supervision, X.C.; project administration, X.C.; resources, X.C. All authors have read and agreed to the published version of the manuscript.

Funding: This research was funded by the central government guides local science and technology development funding—Jilin Province basic research special project, grant number 202002046JC.

Conflicts of Interest: The authors declare no conflict of interest.

References

1. Bertie, J.E.; Lan, Z. Infrared intensities of liquids XX: The intensity of the OH Stretching Band of liquid water revisited, and the best current values of the optical constants of H_2O(l) at 25 °C between 15,000 and 1 cm^{-1}. *Appl. Spectrosc.* **1996**, *50*, 1047–1057. [CrossRef]
2. Kintz, G.J.; Allen, R.; Esterowitz, L. Cw and pulsed 2.8 μm laser emission from diode-pumped Er^{3+}:$LiYF_4$ at room temperature. *Appl. Phys. Lett.* **1987**, *50*, 1553–1555. [CrossRef]
3. Gebbie, H.A.; Harding, W.R.; Hilsum, C.; Pryce, A.W.; Roberts, V. Atmospheric transmission in the 1 to 14 μm region. *Proc. R. Soc. Lond. Ser. A Math. Phys. Sci.* **1951**, *206*, 87–107. [CrossRef]
4. Sorokina, I.T.; Vodopyanov, K.L. *Solid-State Mid-Infrared Laser Sources*; Springer: Berlin/Heidelberg, Germany, 2003.
5. Zajac, A.; Skorczakowski, M.; Swiderski, J.; Nyga, P. Electrooptically Q-switched mid-infrared Er:YAG laser for medical applications. *Opt. Express* **2004**, *12*, 5125–5130. [CrossRef] [PubMed]
6. Vagdouti, T.; Theodoridis, C.; Tseleki, G.; Vouros, I. Long-term clinical outcomes of Er:YAG or Er,Cr:YSGG lasers utilized as monotherapy or as adjuncts to mechanical therapy in the treatment of chronic periodontitis: A systematic review. *Lasers Dent. Sci.* **2023**, *7*, 1–15. [CrossRef]
7. Svejkar, R.; Šulc, J.; Jelínková, H.; Kubeček, V.; Ma, W.; Jiang, D.; Wu, Q.; Su, L. Diode-pumped Er:SrF_2 laser tunable at 2.7 μm. *Opt. Mater. Express* **2018**, *8*, 1025–1030. [CrossRef]
8. Fedorov, V.; Mirov, S.; Gallian, A.; Badikov, D.; Frolov, M.; Korostelin, Y.; Kozlovsky, V.; Landman, A.; Podmar'Kov, Y.; Akimov, V.; et al. 3.77–5.05 μm tunable solid-state lasers based on Fe^{2+}-doped ZnSe crystals operating at low and room temperatures. *IEEE J. Quantum Elect.* **2010**, *42*, 907–917. [CrossRef]
9. Sanamyan, T.; Simmons, J.; Dubinskii, M. Efficient cryo-cooled 2.7 μm Er^{3+}:Y_2O_3 ceramic laser with direct diode pumping of the upper laser level. *Laser Phys. Lett.* **2010**, *7*, 569–572. [CrossRef]
10. Fedorov, V.; Martyshkin, D.; Karki, K.; Mirov, S. Q-switched and gain-switched Fe:ZnSe lasers tunable over 3.60–5.15 μm. *Opt. Express* **2019**, *27*, 13934–13941. [CrossRef]
11. Desurvire, E. *Erbium-Doped Fiber Amplifiers*; John Wiley and Sons: New York, NY, USA, 1994.
12. Kaminskii, A.A. *Laser Crystals*; Springer: Berlin/Heidelberg, Germany, 1990.
13. Dinerman, B.J.; Moulton, P.F. 3 μm cw laser operations in erbium-doped YSGG, GGG, and YAG. *Opt. Lett.* **1994**, *19*, 1143–1145. [CrossRef]
14. Georgescu, S.; Glynn, T.; Sherlock, R.; Lupei, V. Concentration quenching of the $^4I_{9/2}$ level of Er^{3+} in laser crystals. *Opt. Commun.* **1994**, *106*, 75–78. [CrossRef]
15. Lupei, V.; Georgescu, S.; Florea, V. On the dynamics of population inversion for 3 μm Er^{3+} lasers. *IEEE J. Quantum Elect.* **1993**, *29*, 426–434. [CrossRef]
16. Lupei, V.; Georgescu, S. Erbium three-micron laser emission as an up-conversion system. *Opt. Eng.* **1996**, *35*, 1265–1272. [CrossRef]
17. Moulton, P.; Manni, J.; Rines, G. Spectroscopic and laser characteristics of Er,Cr:YSGG. *IEEE J. Quantum Elect.* **1988**, *24*, 960–973. [CrossRef]
18. Feng, S.; Liu, C.; Zhu, J.; Xu, Y.; Xiao, X.; Guo, H. Realizing particle population inversion of 2.7 μm emission in heavy Er^{3+}/Pr^{3+} co-doped low hydroxyl fluorotellurite glass for mid-infrared laser. *Ceram. Int.* **2023**, *49*, 20372–20380. [CrossRef]
19. Schäfer, M.C.; Petter, M.; Hartenbach, I.; Locke, R.J.C.; Zhang, S.; Wickleder, C.; Schleid, T. Luminescence properties of $Y_3F[Si_3O_{10}]$:Ln^{3+} (Ln = Eu, Tb, Er) with thalenite-type host lattice and crystal structure of $Tm_3F[Si_3O_{10}]$. *Crystals* **2023**, *13*, 511. [CrossRef]

20. Zhang, Y.; Hu, S.; Tian, T.; Xiao, X.; Chen, Y.; Zhang, Y.; Xu, J. Growth and spectral properties of Er^{3+} and Yb^{3+} co-doped bismuth silicate single crystal. *Crystals* **2022**, *12*, 1532. [CrossRef]
21. Georgescu, S.; Lupei, V.; Glynn, T.; Sherlock, R. Spectroscopic determination of the figures of merit for 3 μm Er^{3+} lasers. *J. Lumin.* **1994**, *60–61*, 241–244. [CrossRef]
22. Tikerpae, M.; Jackson, S.D.; King, T.A. Theoretical comparison of Er^{3+} doped crystal lasers. *J. Mod. Opt.* **1998**, *45*, 1269–1284. [CrossRef]
23. Švejkar, R.; Šulc, J.; Jelínková, H. Er-doped crystalline active media for ~3 μm diode-pumped lasers. *Prog. Quantum. Electron.* **2020**, *74*, 100276. [CrossRef]
24. Švejkar, R.; Šulc, J.; Boháček, P.; Němec, M.; Jelínková, H.; Trunda, B.; Havlák, L.; Nikl, M.; Jurek, K. Influence of Er^{3+} concentration in Er:GGAG crystal on spectroscopic and laser properties. *J. Alloys Compd.* **2023**, *941*, 168964. [CrossRef]
25. Tang, K.; Yingming, S.; Gai, J.; Pan, Z. Evaluation of growth, thermal, and spectroscopic properties of Er^{3+} doped CLNGG crystals for Use in 2.7 μm Laser. *Crystals* **2021**, *11*, 126. [CrossRef]
26. Zhong, K. Laser performance of neodymium- and erbium-doped GYSGG crystals. *Crystals* **2019**, *9*, 220. [CrossRef]
27. Shterengas, L.; Liang, R.; Kipshidze, G.; Hosoda, T.; Belenky, G.; Bowman, S.S.; Tober, R.L. Cascade type-I quantum well diode lasers emitting 960 mW near 3 μm. *Appl. Phys. Lett.* **2014**, *105*, 161112. [CrossRef]
28. Iwakuni, K.; Porat, G.; Bui, T.Q.; Bjork, B.J.; Schoun, S.B.; Heckl, O.H.; Fermann, M.E.; Ye, J. Phase-stabilized 100 mW frequency comb near 10 μm. *Appl. Phys. B* **2018**, *124*, 128. [CrossRef] [PubMed]
29. Lv, Z.; Shen, Y.; Zong, N.; Bian, Q.; Wang, E.-P.; Chang, J.-Q.; Bo, Y.; Cui, D.-F.; Peng, Q.-J. 1.53 W all-solid-state nanosecond pulsed mid-infrared laser at 6.45 μm. *Opt. Lett.* **2022**, *47*, 1359–1362. [CrossRef]
30. Hemming, A.; Richards, J.; Davidson, A.; Carmody, N.; Bennetts, S.; Simakov, N.; Haub, J. 99 W mid-IR operation of a ZGP OPO at 25% duty cycle. *Opt. Express* **2013**, *21*, 10062–10069. [CrossRef]
31. Lippert, E.; Fonnum, H.; Haakestad, M.W. Laser source with high pulse energy at 3–5 m and 8–12 m based on nonlinear conversion in $ZnGeP_2$. In Proceedings of the Technologies for Optical Countermeasures XI; and High-Power Lasers 2014: Technology and Systems, Amsterdam, The Netherlands, 22–25 September 2014. [CrossRef]
32. Aydin, Y.O.; Fortin, V.; Vallée, R.; Bernier, M. Towards power scaling of 2.8 μm fiber lasers. *Opt. Lett.* **2018**, *43*, 4542–4545. [CrossRef]
33. Shen, Y.; Wang, Y.; Zhu, F.; Ma, L.; Zhao, L.; Chen, Z.; Wang, H.; Huang, C.; Huang, K.; Feng, G. 200 μJ, 13 ns Er:ZBLAN mid-infrared fiber laser actively Q-switched by an electro-optic modulator. *Opt. Lett.* **2021**, *46*, 1141–1144. [CrossRef]
34. Yu, L.; Liang, J.; Huang, S.; Wang, J.; Wang, J.; Luo, X.; Yan, P.; Dong, F.; Liu, X.; Lue, Q.; et al. Average-power (4.13 W) 59 fs mid-infrared pulses from a fluoride fiber laser system. *Opt. Lett.* **2022**, *47*, 2562–2565. [CrossRef]
35. Wei, C.; Luo, H.; Shi, H.; Lyu, Y.; Zhang, H.; Liu, Y. Widely wavelength tunable gain-switched Er^{3+}-doped ZBLAN fiber laser around 2.8 μm. *Opt. Express* **2017**, *25*, 8816. [CrossRef] [PubMed]
36. Lancaster, D.G.; Gross, S.; Ebendorff-Heidepriem, H.; Withford, M.J.; Monro, T.M.; Jackson, S.D. Efficient 2.9 μm fluorozirconate glass waveguide chip laser. *Opt. Lett.* **2013**, *38*, 2588–2591. [CrossRef] [PubMed]
37. Jia, Y.J.Y.; Chen, F.C.F. Compact solid-state waveguide lasers operating in the pulsed regime: A review. *Chin. Opt. Lett.* **2019**, *17*, 012302.
38. Grivas, C. Optically pumped planar waveguide lasers, part I: Fundamentals and fabrication techniques. *Prog. Quantum. Electron.* **2011**, *35*, 159–239. [CrossRef]
39. Grivas, C. Optically pumped planar waveguide lasers: Part II: Gain media, laser systems, and applications. *Prog. Quantum. Electron.* **2016**, *45/46*, 3–160. [CrossRef]
40. Kaminskii, A.A.; Butaeva, T.I.; Ivanov, A.O.; Mochalov, I.V.; Petrosian, A.G.; Rogov, G.I.; Fedorov, V.A. New data on stimulated emission of crystals containing Er^{3+} and Ho^{3+} ions. *Sov. Tech. Phys. Lett.* **1976**, *2*, 308–310.
41. Georgescu, S.; Lupei, V.; Ursu, I. The role of cross-relaxation mechanisms in the quasistationary generation regime of YAG:Er laser. *Rev. Roum. Phys.* **1986**, *31*, 857–864.
42. Chou, H.; Jenssen, H.P. Up-conversion Processes in Er-activated Solid State Laser Materials. In Proceedings of the Advanced Solid State Lasers, Cape Cod, MA, USA, 1 May 1989. [CrossRef]
43. Zhekov, V.I.; Lobachev, V.A.; Murina, T.M.; Prokhorov, A.M. Cooperative phenomena in yttrium erbium aluminum garnet crystals. *Sov. J. Quantum Electron.* **2007**, *14*, 128–130. [CrossRef]
44. Bagdasarov, K.S.; Zhekov, V.I.; Lobachev, V.A.; Manenkov, A.A.; Murina, T.M.; Prokhorov, A.M. Cross-relaxation YAG:Er^{3+} laser. *Izv. Akad. Nauk SSSR Ser. Fiz.* **1984**, *48*, 1765–1770.
45. Georgescu, S.; Lupei, V.; Lupei, A.; Zhekov, V.; Murina, T.; Studenikin, M. Concentration effects on the up-conversion from the $^4I_{13/2}$ level of Er^{3+} in YAG. *Opt. Commun.* **1991**, *81*, 186–192. [CrossRef]
46. Koechner, W. *Solid-State Laser Engeneering*; Springer: Berlin/Heidelberg, Germany, 2006.
47. Hu, L.; Sun, D.; Zhang, H.; Luo, J.; Quan, C.; Han, Z.; Dong, K.; Chen, Y.; Cheng, M. Diode end-pumped 1.37W Er:YSGG continuous-wave laser around 2.8 μm. *IEEE Photon. Technol. Lett.* **2021**, *33*, 611–614. [CrossRef]
48. Lupei, V. ER^{3+} emission in garnets: Multisites, energy transfer and quantum efficiency. *Opt. Mater.* **2002**, *19*, 95–107. [CrossRef]
49. Kränkel, C. Rare-earth-doped sesquioxides for diode-pumped high-power lasers in the 1-, 2-, and 3-μm spectral range. *IEEE J. Sel. Top. Quantum Electron.* **2014**, *21*, 250–262. [CrossRef]

50. Hu, L.; Sun, D.; Luo, J.; Zhang, H.; Zhao, X.; Quan, C.; Han, Z.; Dong, K.; Cheng, M.; Yin, S. Effect of Er^{3+} concentration on spectral characteristic and 2.79 μm laser performance of Er:YSGG crystal. *J. Lumin.* **2020**, *226*, 250–262. [CrossRef]
51. Ma, W.; Su, L.; Xu, X.; Wang, J.; Jiang, D.; Zheng, L.; Fan, X.; Li, C.; Liu, J.; Xu, J. Effect of erbium concentration on spectroscopic properties and 2.79 μm laser performance of Er:CaF_2 crystals. *Opt. Mater. Express* **2016**, *6*, 409–415. [CrossRef]
52. Quan, C.; Sun, D.; Zhang, H.; Luo, J.; Hu, L.; Han, Z.; Qiao, Y.; Dong, K.; Chen, Y.; Cheng, M. Growth, spectroscopy and high-power laser operation of Er:YAP crystal with different Er^{3+} concentrations. *J. Lumin.* **2022**, *251*, 119122. [CrossRef]
53. Matulić, N.; Bago, I.; Sušić, M.; Gjorgievska, E.; Knežević, A.K.; Gabrić, D. Comparison of Er:YAG and Er,Cr:YSGG laser in the treatment of oral leukoplakia lesions refractory to the local retinoid therapy. *Photobiomodul. Photomed. Laser Surg.* **2019**, *37*, 362–368. [CrossRef]
54. Harashima, T.; Kinoshita, J.-I.; Kimura, Y.; Brugnera, A.; Zanin, F.; Pecora, J.D.; Matsumoto, K.; Hossain, M.; Nakamura, Y.; Yamada, Y.; et al. Morphological comparative study on ablation of dental hard tissues at cavity preparation by Er:YAG and Er,Cr:YSGG lasers. *Photomed. Laser Surg.* **2005**, *23*, 52–55. [CrossRef]
55. Wang, K.; Gao, C.; Lin, Z.; Wang, Q.; Gao, M.; Huang, S.; Chen, C. 1645 nm coherent Doppler wind lidar with a single-frequency Er:YAG laser. *Opt. Express* **2020**, *28*, 14694–14704. [CrossRef]
56. Sanamyan, T. Efficient cryogenic mid-IR and eye-safe Er:YAG laser. *J. Opt. Soc. Am. B* **2016**, *33*, D1–D6. [CrossRef]
57. Ter-Gabrielyan, N.; Dubinskii, M.; Newburgh, G.A.; Michael, A.; Merkle, L.D. Temperature dependence of a diode-pumped cryogenic Er:YAG laser. *Opt. Express* **2009**, *17*, 7159–7169. [CrossRef] [PubMed]
58. Wang, S.; Tian, Y.; Qu, B.; Zhu, Z.; Hui, Y.; Lei, H.; Li, Q. High slope efficiency 3 μm Er:YAG cyclic cascade pulsed lasers. *Opt. Laser Technol.* **2023**, *158*, 108868. [CrossRef]
59. Wüthrich, S.; Lüthy, W.; Weber, H.P. Comparison of YAG:Er and $YAlO_3$:Er laser crystals emitting near 2.9 μm. *J. Appl. Phys.* **1990**, *68*, 5467–5471. [CrossRef]
60. Chen, D.-W.; Fincher, C.L.; Rose, T.S.; Vernon, F.L.; Fields, R.A. Diode-pumped 1-W continuous-wave Er:YAG 3 μm laser. *Opt. Lett.* **1990**, *24*, 385–387. [CrossRef]
61. Sousa, J.G.; Welford, D.; Foster, J. Efficient 1.5W CW and 9mJ Quasi-CW TEM_{00} Mode Operation of A Compact Diode-Laser-Pumped 2.94μm Er:YAG Laser. In Proceedings of the Solid State Lasers XIX: Technology and Devices, San Francisco, CA, USA, 23–28 January 2010. [CrossRef]
62. Yang, J.; Wang, L.; Wu, X.; Cheng, T.; Jiang, H. High peak power Q-switched Er:YAG laser with two polarizers and its ablation performance for hard dental tissues. *Opt. Express* **2014**, *22*, 15686–15696. [CrossRef] [PubMed]
63. Karki, K.; Fedorov, V.; Martyshkin, D.; Mirov, S. High energy (0.8J) mechanically Q-switched 2.94 μm Er:YAG laser. *Opt. Express* **2021**, *29*, 4287–4295. [CrossRef] [PubMed]
64. Messner, M.; Heinrich, A.; Hagen, C.; Unterrainer, K. High Brightness Diode Pumped Er:YAG Laser System at 2.94 μm with Nearly 1 kW Peak Power. In Proceedings of the Solid State Lasers XXV: Technology and Devices, San Francisco, CA, USA, 13–18 February 2016. [CrossRef]
65. Abbasi, H.; Bernal, L.M.B.; Hamidi, A.; Droneau, A.; Canbaz, F.; Guzman, R.; Jacques, S.L.; Cattin, P.C.; Zam, A. Combined Nd:YAG and Er:YAG lasers for real-time closed-loop tissue-specific laser osteotomy. *Biomed. Opt. Express* **2020**, *11*, 1790–1807. [CrossRef]
66. LLi, Y.-Y.; Dai, T.-Y.; Duan, X.-M.; Guo, C.-F.; Xu, L.-W.; Ju, Y.-L. Fe:ZnSe laser pumped by a 2.93 μm Cr, Er:YAG laser. *Chin. Phys. B* **2019**, *28*, 195–198. [CrossRef]
67. Martyshkin, D.; Karki, K.; Fedorov, V.; Mirov, S. Room temperature, nanosecond, 60 mJ/pulse Fe: ZnSe master oscillator power amplifier system operating at 3.8–5.0 μm. *Opt. Express* **2021**, *29*, 2387–2393. [CrossRef]
68. Nie, H.; Wang, F.; Liu, J.; Yang, K.; Zhang, B.; He, J. Rare-earth ions-doped mid-infrared (2.7–3 μm) bulk lasers: A review. *Chin. Opt. Lett.* **2021**, *19*, 091407. [CrossRef]
69. Arbabzadah, E.A.; Phillips, C.C.; Damzen, M.J. Free-running and Q-switched operation of a diode pumped Er:YSGG laser at the 3μm transition. *Appl. Phys. B* **2013**, *111*, 333–339. [CrossRef]
70. Wang, J.; Cheng, T.; Wang, L.; Yang, J.; Sun, D.; Yin, S.; Wu, X.; Jiang, H. Compensation of strong thermal lensing in an LD side-pumped high-power Er:YSGG laser. *Laser Phys. Lett.* **2015**, *12*, 105004. [CrossRef]
71. Chen, G.; Li, B.; Zhao, S.; Yuan, L.; Wei, L. High-weight LD pump Er:YSGG solid laser. *Laser Infrared* **2019**, *49*, 956–960.
72. Hu, Q.; Nie, H.; Mu, W.; Yin, Y.; Zhang, J.; Zhang, B.; He, J.; Jia, Z.; Tao, X. Bulk growth and an efficient mid-IR laser of high-quality Er:YSGG crystals. *Laser Phys. Lett.* **2019**, *21*, 1928–1933. [CrossRef]
73. Ye, X.; Xu, X.; Ren, H.; Zhang, B.; Zhang, L.; Wei, X.; Wan, M.; He, T. Enhanced high-slope-efficiency and high-power LD side-pumped Er:YSGG laser. *Appl. Opt.* **2019**, *58*, 9949–9954. [CrossRef]
74. Ye, X.; Xu, X.; Ren, H.; Zhang, B.; Zhang, L.; Wei, X.; Fan, G. Study of LD side-pumped two-rod Er:YSGG mid-infrared laser with 61-W output power. *Opt. Commun.* **2022**, *507*, 127608. [CrossRef]
75. Mitrokhin, V.P.; Savvin, A.D.; Simonova, V.; Sirotkin, A.A.; Firsov, K.N.; Dormidonov, A.E.E. Er:YAG, Er:Cr: YSGG and Ho:Yb:Cr: YSGG lasers with high power diode pumping. *Kvantovaya Elektron.* **2022**, *52*, 597–603.
76. Malekafzali, B.; Asnaashari, M.; Javadi, F. Comparison of marginal microleakage of flowable composite restorations in primary canine teeth prepared with high-speed diamond bur, Er:YAG laser and Er,Cr:YSGG laser. *Laser Ther.* **2017**, *26*, 195–202. [CrossRef]
77. Sorokin, P.P.; Stevenson, M.J. Stimulated infrared emission from trivalent uranium. *Phys. Rev. Lett.* **1960**, *5*, 557–559. [CrossRef]

78. Robinson, M.; Devor, D.P. Thermal switching of laser emission of Er^{3+} at 2.69 μm and Tm^{3+} at 1.86 μm in mixed crystals of CaF_2:ErF_3:TmF_3. *Appl. Phys. Lett.* **1967**, *10*, 167–170. [CrossRef]
79. Silversmith, A.J.; Lenth, W.; Macfarlane, R.M. Green infrared-pumped erbium upconversion laser. *Appl. Phys. Lett.* **1987**, *51*, 1977–1979. [CrossRef]
80. Basiev, T.T.; Orlovskii, Y.V.; Polyachenkova, M.V.; Fedorov, P.P.; Kuznetsov, S.V.; Konyushkin, V.A.; Osiko, V.V.; Alimov, O.K.; Dergachev, A.Y. Continuously tunable cw lasing near 2.75 μm in diode-pumped Er^{3+}:SrF_2 and Er^{3+}:CaF_2 crystals. *Quantum Electron.* **2006**, *36*, 591. [CrossRef]
81. Šulc, J.; Němec, M.; Švejkar, R.; Jelínková, H.; Doroshenko, M.E.; Fedorov, P.P.; Osiko, V.V. Diode-pumped Er:CaF_2 ceramic 2.7 μm tunable laser. *Opt. Lett.* **2013**, *38*, 3406–3409. [CrossRef] [PubMed]
82. Fan, M.; Li, T.; Zhao, J.; Zhao, S.; Li, G.; Yang, K.; Su, L.; Ma, H.; Kränkel, C. Continuous wave and ReS_2 passively Q-switched Er:SrF_2 laser at ∼3 μm. *Opt. Lett.* **2018**, *43*, 1726–1729. [CrossRef]
83. Zhao, Y.-H.; Zong, M.-Y.; Dong, J.-H.; Zhang, Z.; Liu, J.-J.; Liu, J.; Su, L.-B. Mid-infrared Lightly Er^{3+} doped CaF_2 Laser under Acousto-optical Modulation. *Chin. Phys. B* **2022**, *32*, 034203. [CrossRef]
84. Ma, W.; Qian, X.; Wang, J.; Liu, J.; Fan, X.; Liu, J.; Su, L.; Xu, J. Highly efficient dual-wavelength mid-infrared CW Laser in diode end-pumped Er:SrF_2 single crystals. *Sci. Rep.* **2016**, *6*, 36635. [CrossRef]
85. Švejkar, R.; Šulc, J.; Němec, M.; Jelínková, H.; Doroshenko, M.E.; Nakladov, A.N.; Osiko, V.V. Effect of Cryogenic Temperature on Spectroscopic and Laser Properties of Er;La:SrF_2-CaF_2 Crystal. In Proceedings of the Solid State Lasers XXV: Technology and Devices, San Francisco, CA, USA, 13–18 February 2016. [CrossRef]
86. Li, C.; Liu, J.; Jiang, S.; Xu, S.; Ma, W.; Wang, J.; Xu, X.; Su, L. 2.8 μm passively Q-switched Er:CaF_2 diode-pumped laser. *Opt. Mater. Express* **2016**, *6*, 1570–1575. [CrossRef]
87. Su, L.; Guo, X.; Jiang, D.; Wu, Q.; Qin, Z.; Xie, G. Highly-efficient mid-infrared CW laser operation in a lightly-doped 3 at.% Er:SrF_2 single crystal. *Opt. Express* **2018**, *26*, 5558–5563. [CrossRef]
88. Liu, J.; Feng, X.; Fan, X.; Zhang, Z.; Zhang, B.; Liu, J.; Su, L. Efficient continuous-wave and passive Q-switched mode-locked Er^{3+}:CaF_2–SrF_2 lasers in the mid-infrared region. *Opt. Lett.* **2018**, *43*, 2418–2421. [CrossRef]
89. Guo, L.; Wang, M.; Zhang, Y.; Zhang, S.; Zhong, K.; Zhao, Q.; Teng, L.; Wang, X.; Yao, J. Mid-Infrared Dual-Wavelength Passively Q-Switched Er:SrF_2 Laser by $CsPbCl_3$ Quantum Dots Absorber. *Crystals* **2022**, *12*, 1265. [CrossRef]
90. Liao, J.; Chen, Q.; Niu, X.; Zhang, P.; Tan, H.; Ma, F.; Li, Z.; Zhu, S.; Hang, Y.; Yang, Q.; et al. Energy Transfer and Cross-Relaxation Induced Efficient 2.78 μm Emission in Er^{3+}/Tm^{3+}:PbF_2 mid-Infrared Laser Crystal. *Crystals* **2021**, *11*, 1024. [CrossRef]
91. Messner, M.; Heinrich, A.; Unterrainer, K. High-energy diode side-pumped Er:$LiYF_4$ laser. *Appl. Opt.* **2018**, *57*, 1497–1503. [CrossRef] [PubMed]
92. Gao, W.; Wang, R.; Han, Q.; Dong, J.; Yan, L.; Zheng, H. Tuning Red Upconversion Emission in Single $LiYF_4$:Yb^{3+}/Ho^{3+} Microparticle. *J. Phys. Chem. C* **2015**, *119*, 2349–2355. [CrossRef]
93. Jensen, T.; Diening, A.; Huber, G.; Chai, B. A Diode Pumped 1.1W cw Er:YLF Laser At 2.8 μm. In Proceedings of the Conference on Lasers and Electro-Optics, Baltimore, MD, USA, 21–26 May 1995.
94. Wyss, C.; Lüthy, W.; Weber, H.; Rogin, P.; Hulliger, J. Emission properties of an optimised 2.8 μm Er^{3+}:YLF laser. *Opt. Commun.* **1997**, *139*, 215–218. [CrossRef]
95. Dergachev, A.; Moulton, P.F. Tunable CW Er:YLF Diode-Pumped Laser. In Proceedings of the Advanced Solid-State Photonics, San Antonio, TX, USA, 2–5 February 2003.
96. Inochkin, M.V.; Nazarov, V.V.; Sachkov, D.Y.; Khloponin, L.V.; Khramov, V.Y. Dynamics of the lasing spectrum of a 3-μm Er:YLF laser with semiconductor pumping. *J. Opt. Technol.* **2009**, *76*, 720–724. [CrossRef]
97. Inochkin, M.V.; Nazarov, V.V.; Sachkov, D.Y.; Khloponin, L.V.; Khramov, V.Y. The dynamics of the emission spectrum of an Er:YLF laser in the pulsed-periodic operating regime. *J. Opt. Technol.* **2010**, *77*, 413–416. [CrossRef]
98. Inochkin, M.V.; Korostelin, Y.V.; Landman, A.I.; Nazarov, V.V.; Sachkov, D.Y.; Podmar'kov, Y.P.; Frolov, M.P.; Khloponin, L.V.; Khramov, V.Y. A compact Er:YLF laser with a passive Fe^{2+}:ZnSe shutter. *J. Opt. Technol.* **2012**, *79*, 337–339. [CrossRef]
99. Fedorov, N.; Inochkin, M.; Khloponin, L.; Khramov, V.; Nazarov, V.; Sachkov, D. Multiwave diode pumped Q-switch Er:YLF laser. In Proceedings of the 2014 International Conference Laser Optics, St. Petersburg, Russia, 30 June–4 July 2014. [CrossRef]
100. Messner, M.; Heinrich, A.; Hagen, C.; Unterrainer, K. Acousto-optically Q-switched diode side-pumped Er:YLF laser generating 50kW peak power in 70ns pulses. In Proceedings of the Solid State Lasers XXVIII: Technology and Devices, San Francisco, CA, USA, 2–7 February 2019. [CrossRef]
101. Ter-Gabrielyan, N.; Fromzel, V. Cascade generation at 1.62, 1.73 and 2.8 μm in the Er:YLF Q-switched laser. *Opt. Express* **2019**, *27*, 20199–20210. [CrossRef]
102. Švejkar, R.; Šulc, J.; Němec, M.; Jelínková, H. Compact diode-pumped CW and Q-switched 2.8 μm Er:YLF laser. *J. Opt. Soc. Am. B* **2021**, *38*, B26–B29. [CrossRef]
103. Pushkin, A.; Slovinsky, I.A.; Shakirov, A.A.; Shavelev, A.; Potemkin, F.V. Diode-side-pumped watt-level high-energy Q-switched mid-IR Er:YLF laser. *Opt. Lett.* **2021**, *46*, 5465–5468. [CrossRef]
104. Sanamyan, T.; Dubinskii, M. Er^{3+}-Doped Diode-Pumped Ceramic Laser Delivers 14 W CW at 2.7 μm. In Proceedings of the CLEO: Science and Innovations, Baltimore, MD, USA, 1–6 May 2011. [CrossRef]
105. Sanamyan, T.; Kanskar, M.; Xiao, Y.; Kedlaya, D.; Dubinskii, M. High power diode-pumped 2.7-μm Er^{3+}:Y_2O_3 laser with nearly quantum defect-limited efficiency. *Opt. Express* **2011**, *19*, A1082–A1087. [CrossRef] [PubMed]

106. Fleischman, Z.D.; Sanamyan, T. Spectroscopic analysis of Er^{3+}:Y_2O_3 relevant to 2.7μm mid-IR laser. *Opt. Mater. Express* **2016**, *6*, 3109–3118. [CrossRef]
107. Sanamyan, T. Diode pumped cascade Er:Y_2O_3 laser. *Laser Phys. Lett.* **2015**, *12*, 125804. [CrossRef]
108. Wang, L.; Huang, H.; Shen, D.; Zhang, J.; Chen, H.; Tang, D. Diode-pumped high power 2.7 μm Er: Y_2O_3 ceramic laser at room temperature. *Opt. Mater.* **2022**, *71*, 70–73. [CrossRef]
109. Ding, M.; Li, X.; Wang, F.; Shen, D.; Wang, J.; Tang, D.; Zhu, H. Power scaling of diode-pumped Er:Y_2O_3 ceramic laser at 2.7 μm. *Appl. Phys. Express* **2022**, *15*, 062004. [CrossRef]
110. Qin, Z.; Xie, G.; Zhang, J.; Ma, J.; Yuan, P.; Qian, L. Continuous-Wave and Passively Q-Switched Er:Y_2O_3 Ceramic Laser at 2.7 μm. *Int. J. Opt.* **2018**, *2018*, 3153614. [CrossRef]
111. Peters, V.; Fornasiero, L.; Mix, E.; Diening, A.; Petermann, K.; Huber, G. Spectroscopic Characterization And Diode-Pumped Laser Action At 2.7 μm of Er:Lu_2O_3. In Proceedings of the European Conference on Lasers and Electro-Optics, Glasgow, UK, 14–18 September 1998. [CrossRef]
112. Li, T.; Beil, K.; Krankel, C.; Brandt, C.; Huber, G. Laser performance of highly doped Er:Lu_2O_3 at 2.8μm. In Proceedings of the Advanced Solid-State Photonics, San Diego, CA, USA, 29 January–1 February 2012. [CrossRef]
113. Li, T.; Beil, K.; Kränkel, C.; Huber, G. Efficient high-power continuous wave Er:Lu_2O_3 laser at 2.85 μm. *Opt. Lett.* **2012**, *37*, 2568–2570. [CrossRef]
114. Yao, W.; Uehara, H.; Tokita, S.; Chen, H.; Konishi, D.; Murakami, M.; Yasuhara, R. LD-pumped 2.8 μm Er:Lu_2O_3 ceramic laser with 6.7 W output power and >30% slope efficiency. *Appl. Phys. Express.* **2020**, *14*, 012001. [CrossRef]
115. Wang, L.; Huang, H.; Shen, D.; Zhang, J.; Tang, D. High Power and Short Pulse Width Operation of Passively Q-Switched Er:Lu_2O_3 Ceramic Laser at 2.7 μm. *Appl. Sci.* **2018**, *8*, 801. [CrossRef]
116. Uehara, H.; Tokita, S.; Kawanaka, J.; Konishi, D.; Murakami, M.; Yasuhara, R. A passively Q-switched compact Er:Lu_2O_3 ceramics laser at 2.8 μm with a graphene saturable absorber. *Appl. Phys. Express* **2019**, *12*, 022002. [CrossRef]
117. Stalder, M.; Lüthy, W. Polarisation of 3 μm laser emission in $YAlO_3$:Er. *Opt. Commun.* **1987**, *61*, 274–276. [CrossRef]
118. Zeng, R.R.; Shen, H.Y.; Huang, C.N.; Zhou, Y.P.; Yu, G.F.; Zeng, Z.D.; Lu, J.; Ye, Q.J. A 2.7 μm Er: YAP laser. *Chin. J. Lasers* **1990**, *17*, 60–62.
119. Švejkar, R.; Šulc, J.; Němec, M.; Jelínková, H.; Nejezchleb, K.; Čech, M. Temperature Influence on Spectroscopic Properties and 2.7 μm Lasing of Er:YAP Crystal. In Proceedings of the Solid State Lasers XXVII: Technology and Devices, San Francisco, CA, USA, 27 January–1 February 2018. [CrossRef]
120. Quan, C.; Sun, D.; Luo, J.; Zhang, J.; Fang, Z.; Zhao, X.; Hu, L.; Cheng, M.; Zhang, Q.; Yin, S. 2.7 μm dual-wavelength laser performance of LD end-pumped Er:YAP crystal. *Opt. Express* **2018**, *26*, 28421–28428. [CrossRef]
121. Kawase, H.; Yasuhara, R. 2.92 μm high-efficiency continuous-wave laser operation of diode-pumped Er:YAP crystal at room temperature. *Opt. Express* **2019**, *27*, 12213–12220. [CrossRef]
122. Kawase, H.; Uehara, H.; Chen, H.; Yasuhara, R. Passively Q-switched 2.9 μm Er:YAP single crystal laser using graphene saturable absorber. *Appl. Phys. Express* **2019**, *12*, 102006. [CrossRef]
123. Yao, Y.; Cui, N.; Wang, Q.; Dong, L.; Liu, S.; Sun, D.; Zhang, H.; Li, D.; Zhang, B.; He, J. Highly efficient continuous-wave and $ReSe_2$ Q-switched ∼3 μm dual-wavelength Er:YAP crystal lasers. *Opt. Lett.* **2019**, *44*, 2839–2842. [CrossRef]
124. Yao, W.; Uehara, H.; Kawase, H.; Chen, H.; Yasuhara, R. Highly efficient Er:YAP laser with 6.9W of output power at 2920 nm. *Opt. Express* **2020**, *28*, 19000–19007. [CrossRef] [PubMed]
125. Yao, W.; Uehara, H.; Li, E.; Yasuhara, R. Power-scalable two-wavelength pumped Er:YAP laser at 2.9 μm. *Opt. Laser. Technol.* **2022**, *152*, 108073. [CrossRef]
126. Buryi, M.; Gaston-Bellegarde, A.M.; Pejchal, J.; Levchenko, F.; Remeš, Z.; Ridzoňová, K.; Babin, V.; Chertopalov, S. The role of Er^{3+} content in the luminescence properties of $Y_3Al_5O_{12}$ single crystals: Incorporation into the lattice and defect state creation. *Crystals* **2023**, *13*, 562. [CrossRef]
127. Park, Y.H.; Lee, D.W.; Kong, H.J.; Kim, Y.S. Dynamics of a flashlamp pumped 2.70 μm emission Cr:Er:YSGG laser with an infrared-quartz FTIR shutter. *J Opt. Soc. Am. B* **2008**, *25*, 2123–2129. [CrossRef]
128. Murphy, F.J.; Arbabzadah, E.A.; Bak, A.O.; Amrania, H.; Damzen, M.J.; Phillips, C.C. Optical chopper Q-switching for flashlamp-pumped Er.Cr:YSGG lasers. *Laser. Phys. Lett.* **2015**, *12*, 045802. [CrossRef]
129. Jiang, L.L.; Wu, Z.C.; Cheng, T.Q.; Jiang, H. 79-μm efficient acousto-optic Q switched Er,Cr:YSGG laser with an $LiNbO_3$ crystal modulator. *Opt. Lett.* **2020**, *47*, 6193–6196. [CrossRef] [PubMed]
130. Myoung, N.; Martyshkin, D.V.; Fedorov, V.V.; Mirov, S.B. Energy scaling of 4.3 μm room temperature Fe:ZnSe laser. *Opt. Lett.* **2011**, *36*, 94–96. [CrossRef] [PubMed]

Disclaimer/Publisher's Note: The statements, opinions and data contained in all publications are solely those of the individual author(s) and contributor(s) and not of MDPI and/or the editor(s). MDPI and/or the editor(s) disclaim responsibility for any injury to people or property resulting from any ideas, methods, instructions or products referred to in the content.